

# Floquet prethermalization with lifetime exceeding 90s in a bulk hyperpolarized solid

William Beatrez,<sup>1</sup> Otto Janes,<sup>1</sup> Amala Akkiraju,<sup>1</sup> Arjun Pillai,<sup>1</sup> Alexander Oddo,<sup>1</sup> Paul Reshetikhin,<sup>1</sup> Emanuel Druga,<sup>1</sup> Maxwell McAllister,<sup>1</sup> Mark Elo,<sup>2</sup> Benjamin Gilbert,<sup>3</sup> Dieter Suter,<sup>4</sup> and Ashok Ajoy<sup>1,5,\*</sup>

<sup>1</sup>Department of Chemistry, University of California, Berkeley, Berkeley, CA 94720, USA.

<sup>2</sup>Tabor Electronics Inc. Hatasia 9, Nesher, 3660301, Israel.

<sup>3</sup>Energy Geoscience Division, Lawrence Berkeley National Laboratory, Berkeley, CA 94720, USA.

<sup>4</sup>Fakultät Physik, Technische Universität Dortmund, D-44221 Dortmund, Germany.

<sup>5</sup>Chemical Science Division, Lawrence Berkeley National Laboratory, University of California, Berkeley, Berkeley, CA 94720, USA.

We report the observation of long-lived Floquet prethermal states in a bulk solid composed of dipolar-coupled  $^{13}\text{C}$  nuclei in diamond at room temperature. For precessing nuclear spins prepared in an initial transverse state, we demonstrate Floquet control that prevents their decay over multiple-minute long periods. We observe Floquet prethermal lifetimes  $T_2' \approx 90.9\text{s}$ , extended  $>60,000$ -fold over the nuclear free induction decay times. The spins themselves are continuously interrogated for  $\sim 10\text{min}$ , corresponding to the application of  $\approx 5.8\text{M}$  control pulses. The  $^{13}\text{C}$  nuclei are optically hyperpolarized by lattice Nitrogen Vacancy (NV) centers; the combination of hyperpolarization and continuous spin readout yields significant signal-to-noise in the measurements. This allows probing the Floquet thermalization dynamics with unprecedented clarity. We identify four characteristic regimes of the thermalization process, discerning short-time transient processes leading to the prethermal plateau, and long-time system heating towards infinite temperature. This work points to new opportunities possible via Floquet control in networks of dilute, randomly distributed, low-sensitivity nuclei. In particular, the combination of minutes-long prethermal lifetimes and continuous spin interrogation opens avenues for quantum sensors constructed from hyperpolarized Floquet prethermal nuclei.

**Introduction** – Systems pulled away from thermal equilibrium can exhibit unusual phenomena non-existent or difficult to achieve at equilibrium [1]. For instance, periodically driven quantum systems can display long-lived “Floquet prethermal” regimes due to the emergence of approximately conserved quantities under the effective time-independent Hamiltonian describing the drive [2–6]. For sufficiently large driving frequencies  $\omega$ , much higher than the intrinsic energy scales in the system Hamiltonian (hereafter  $J$ ), these prethermal lifetimes scale exponentially with  $\omega$  [7–10]. Ultimately, however, the system absorbs energy and “heats up” to infinite temperature.

The long-lived prethermal plateau and its stability against perturbations in the drive portends applications for the “Floquet engineering” of quantum states [3, 4]. Fundamentally, the control afforded by periodically driven systems opens avenues to study non-equilibrium phenomena and explore novel dynamic phases of matter, some of which have no equilibrium counterparts [11, 12]. A flurry of theoretical work has recognized Floquet prethermalization under random driving [13], in driven linear chains [9], and even in the classical limit [14]. Experimentally, Floquet prethermalization has been observed in cold-atom [15–17] and NMR systems [18–20]. They demonstrated a characteristic exponential suppression of heating rates with Floquet driving.

In this Letter, we report observation of Floquet prethermal states with lifetimes exceeding 90s at room temperature in a dipolar-coupled ensemble of  $^{13}\text{C}$  nuclei in diamond (see Fig. 1A). These nuclear spins, *randomly* positioned at 1% concentration in the lattice, are optically hyperpolarized by interactions with NV defect centers, which enhances their polarization  $\varepsilon=223$ -fold with respect to the thermal limit (Fig. 1B). When placed in a Bloch transverse state  $\hat{x}$ , these precessing nuclei naturally dephase with free induction decay lifetime  $T_2^* \approx 1.5\text{ms}$ . Under periodic driving, however, we are able to affect a signif-

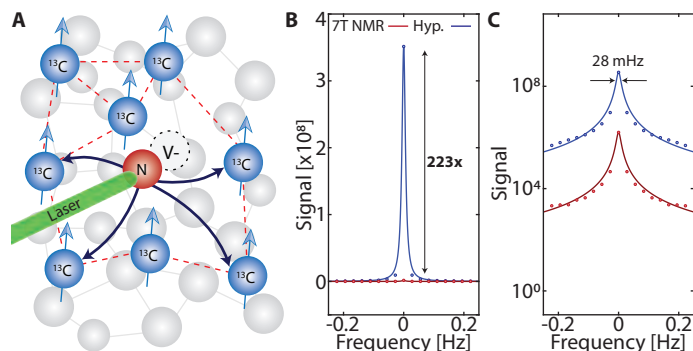


Fig. 1. **System.** (A) Dipolar lattice of  $^{13}\text{C}$  nuclei in diamond. Optically pumped NV centers are employed to hyperpolarize the  $^{13}\text{C}$  nuclei (blue arrows). (B-C) Signal gains from hyperpolarization, demonstrated by comparing *single-shot*  $^{13}\text{C}$  NMR spectra to conventional 7T (thermal) NMR. Data is shown in (B) linear and (C) log scales; line is a fit. Here, optical pumping was for 2min at 36mT, and thermal measurement was taken after 4hrs in the magnet.

icant improvement; the observed Floquet prethermal lifetimes  $T_2' \approx 90.9\text{s}$  constitute a  $>60,000$ -fold extension over  $T_2^*$ . Moreover, with a Floquet drive consisting of  $\approx 5.8\text{M}$  pulses, we are able to continuously probe the thermalization process for up to 573s with high fidelity. This corresponds to  $>10^{10}$  precession cycles of the nuclear spins. Both with respect to the extent of Floquet control applied, and the ultimate transverse spin lifetimes, these values are amongst the largest reported in literature.

A primary contribution in this work is the ability to probe the system thermalization dynamics with high signal-to-noise (SNR). This arises from a combination of hyperpolarization, and improvements in the measurement apparatus that allow sampling the dynamics throughout the Floquet thermalization process (except during the pulses.) This permits a view into the thermalization process with a high degree of clarity, and in a manner not directly accessible in previous experiments. Following theoretical predictions, we identify the four (smoothly

\* ashokaj@berkeley.edu

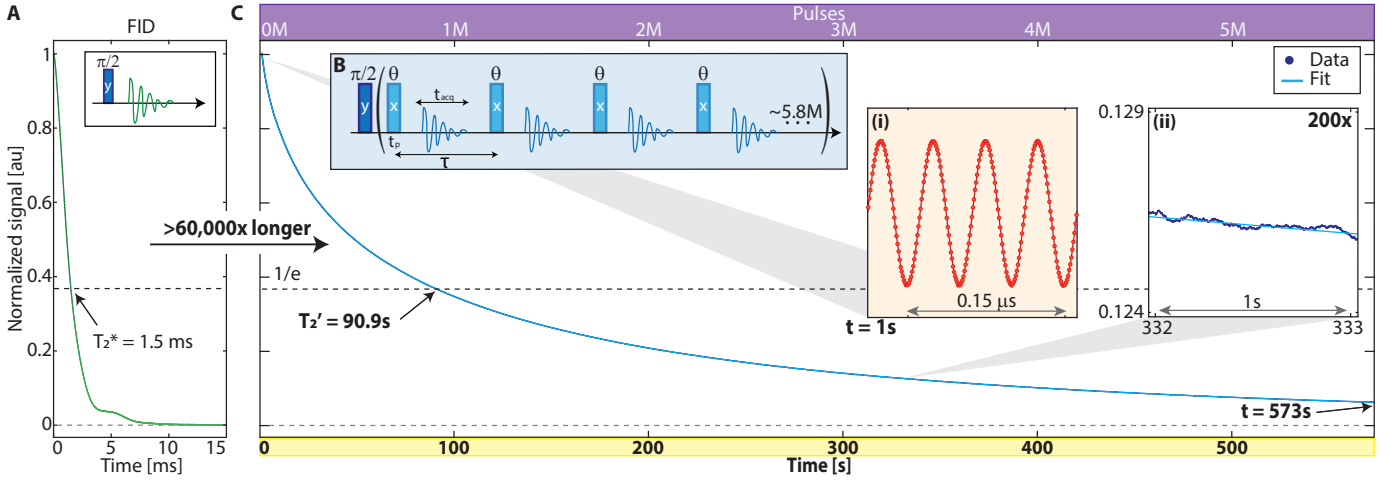


Fig. 2. **Floquet driving and lifetime extension.** (A) Conventional  $^{13}\text{C}$  free induction decay with  $T_2^* \approx 1.5\text{ms}$ . (B) *Floquet drive* consists of a train of  $\vartheta$ -pulses applied spin-locked with the  $^{13}\text{C}$  nuclei. Spins are interrogated in  $t_{\text{acq}}$  windows between the pulses (blue lines), the nuclear precession is sampled every  $1\text{ns}$ . Pulse repetition rate  $\omega = \tau^{-1}$ . (C) *Minutes-long lifetimes* of the transverse state result from the Floquet sequence ( $\vartheta \approx \pi/2$ ). Data (blue points) shows *single-shot* measurement of survival probability in the state  $\rho_I$ , and line is a fit to a sum of five exponentials. Here  $t_{\text{acq}} = 2\mu\text{s}$ ,  $t_p = 40\mu\text{s}$  and  $\tau = 99.28\mu\text{s}$ , and the  $573\text{s}$  period corresponds to  $\approx 5.8\text{M}$  pulses (upper axis). We neglect here the first  $100\text{ms}$  for clarity (see Fig. 3A). *Inset (i)*: Raw data showing measurement of the  $^{13}\text{C}$  spin precession, here at  $1\text{s}$  into the decay. *Inset (ii)*: Data zoomed  $200\times$  in a  $1\text{s}$  window. Using a  $1/e$ -proxy yields  $T_2' \approx 90.9\text{s}$ . This corresponds to a  $>60,000$ -fold extension compared to the FID.

transitioning) regimes — an initial transient to the prethermal plateau, the crossover to unconstrained thermalization and, ultimately, infinite temperature. In the latter regimes, we observe system heating scaling  $\propto \exp(-t^{1/2})$  for a wide range of drive frequencies. The long Floquet prethermal lifetimes here suggests new opportunities in hyperpolarizable spin networks consisting of dilute low-magnetogyric ratio nuclei for quantum sensing [21].

**System** — Diamond  $^{13}\text{C}$  nuclei are distributed with density  $\sim 0.92/\text{nm}^3$ . In a magnetic field  $\mathbf{B}_0$ , the interactions between the nuclei can be represented by the dipolar Hamiltonian,  $\mathcal{H}_{dd} = \sum_{j < k} d_{jk}^{\text{CC}} (3I_{jz}I_{kz} - \vec{I}_j \cdot \vec{I}_k)$ , with a coupling strength  $d_{jk}^{\text{CC}} = \frac{\mu_0 \hbar \gamma_n^2}{4\pi} (3 \cos^2 \vartheta_{jk} - 1) \frac{1}{r_{jk}^3}$ , where  $I$  refer to spin-1/2 Pauli matrices,  $\gamma_n = 10.7\text{MHz/T}$  is the gyromagnetic ratio, and  $\vartheta_{jk} = \cos^{-1} \left( \frac{\mathbf{r}_{jk} \cdot \mathbf{B}_0}{r_{jk} B_0} \right)$  is the angle of the internuclear vector  $\mathbf{r}_{jk}$  to the magnetic field. For the diamond crystal employed in these experiments, the median dipolar coupling  $J = \langle d_{jk}^{\text{CC}} \rangle \approx 663\text{Hz}$  (estimated from Fig. 2A). Furthermore, the sample is oriented with  $\mathbf{B}_0 \parallel [100]$ , such that nearest neighbor (NN)  $^{13}\text{C}$  sites have vector  $\mathbf{r}_{jk}$  oriented at the magic angle, and are hence decoupled. The random  $^{13}\text{C}$  distribution leads to a long tailed distribution in the coupling values, effectively rendering the interaction Hamiltonian *disordered*. In addition, the nuclei are subject to on-site disorder, i.e. local dephasing fields,  $\mathcal{H}_z = \sum_j c_j I_{jz}$ , arising from interactions with paramagnetic impurities (e.g. P1 centers) [22].  $\langle c_j \rangle$  here reflects the strength of the longitudinal P1- $^{13}\text{C}$  hyperfine field [23]; at typical 20ppm P1 concentrations,  $\langle c_j^2 \rangle \approx 0.4[\text{kHz}]^2$  [24]. Apart from the Zeeman contribution  $\gamma_n I_z$ , the net  $^{13}\text{C}$  Hamiltonian is therefore a combination of the interaction and on-site terms,  $\mathcal{H} = \mathcal{H}_{dd} + \mathcal{H}_z$ .

Even before the current resurgence of interest, decades-old NMR experiments had probed thermalization dynamics in

driven nuclear systems [25, 26]. The vast preponderance of NMR experiments have, however, been limited to high- $\gamma_n$  and dense (100% abundant) nuclei such as  $^{19}\text{F}$ ,  $^{31}\text{P}$ , and  $^1\text{H}$  [18, 20]. Instead, we focus attention to dilute networks of insensitive nuclei ( $^{13}\text{C}$ ). They provide a combination of factors critical to establishing Floquet control for long periods — (i) a relatively low  $\|\mathcal{H}_{dd}\|$  compared to networks constructed from sensitive (high- $\gamma_n$ ) nuclei, scaling as  $\eta^{1/2} \gamma_n^2$ , where  $\eta$  is the nuclear enrichment, (ii) a long tailed distribution in couplings, and (iii) long nuclear  $T_1$  (here  $\approx 25\text{min}$ ), significantly higher than many experimental systems, sets a long “memory” time for the nuclear states.

Indeed, these very factors, while attractive for Floquet control [27], make experiments challenging on account of poor sensitivity. Inductively measured nuclear signals scale  $\propto \gamma_n^2$ , with a measurement repetition rate set by  $T_1^{-1}$ , making obtaining reasonable SNR a challenge [28]. We mitigate these difficulties by a combination of hyperpolarization and instrumental advances (allowing continuous sampling). Hyperpolarization is carried out at  $B_{\text{pol}} = 36\text{mT}$  through a method previously described [29, 30]. Measurement throughput is accelerated by  $\approx \frac{1}{2} \varepsilon^2 \left[ T_1(B_0) / T_1(B_{\text{pol}}) \right]^2 \frac{T_2'}{T_2} \gtrsim 10^{10}$  over conventional high-field (FID-based) NMR readout. The overall SNR in a signal such as Fig. 1B-C then exceeds  $10^9$  per shot.

**Floquet control and measurement** — The Floquet driving protocol is described in Fig. 2B. Post polarization, the  $^{13}\text{C}$  nuclei are rotated to transverse axis  $\hat{x}$  on the Bloch sphere, placing them in an initial state  $\rho_I \sim \varepsilon I_x$ . The Floquet drive consists of an equally spaced train of pulses of flip angle  $\vartheta$ . The center-to-center pulse separation is  $\tau [=(\omega/2\pi)^{-1}]$ . After  $N$  pulses, the unitary operator describing its action in the rotating frame can be written as,  $U(N\tau) = [\exp(i\vartheta I_x) \exp(i\mathcal{H}\tau)]^N$ , where we have made a simplifying assumption of  $\delta$ -pulses. The data is sampled after every pulse,  $t_j = j\tau$ , and the evolution can be described by the operation  $U(t) = \prod_{j=1}^N \exp(i\mathcal{H}^{(j)}\tau)$ , where we refer to the

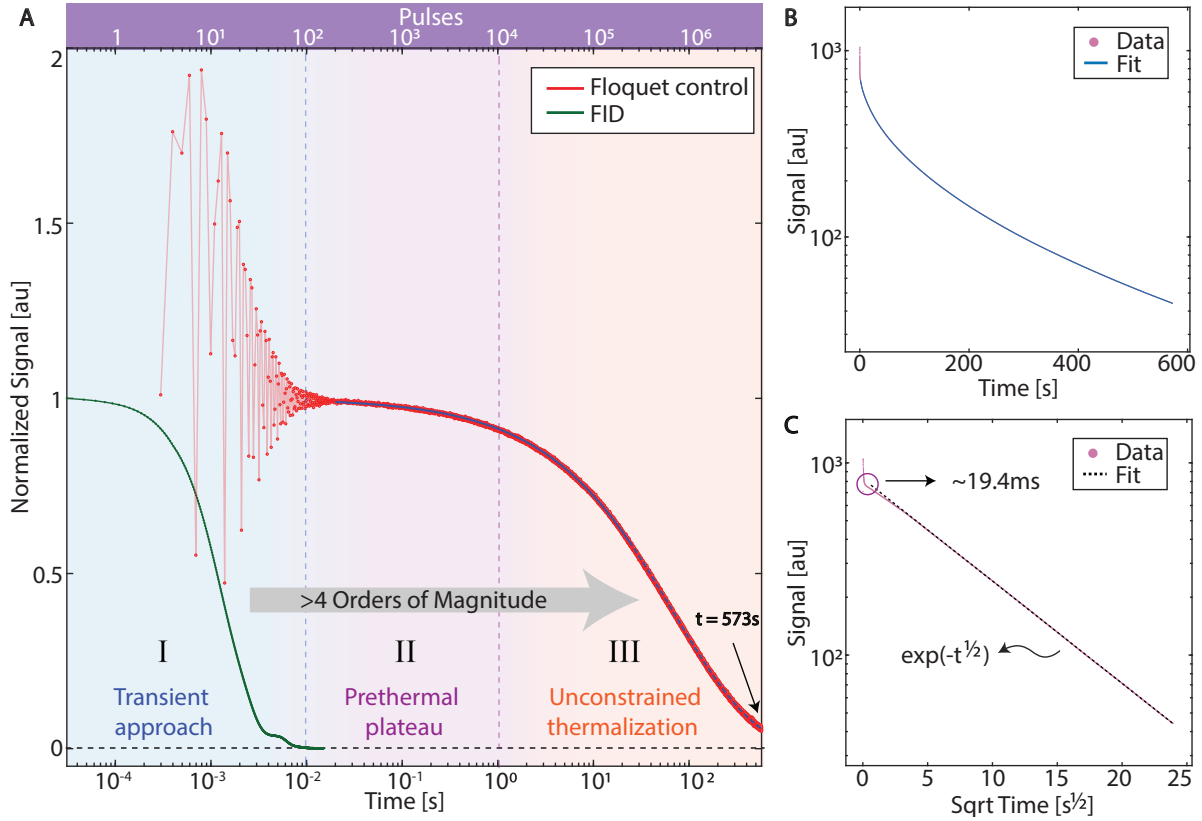


Fig. 3. **Floquet thermalization regimes** (A) *Log-scale* visualization of the full data in Fig. 2C. Points are experiment, there are  $\approx 5.8$ M data points here. Lines are carried out in two segments with solid and dashed lines referring to a stretched exponential with  $\alpha=0.55$  and  $\alpha=0.5$  respectively. Upper axis denotes number of pulses applied, here  $J\tau \approx 0.066$ . Green points are the FID. We observe distinct, yet smoothly transitioning (shaded), thermalization regimes (I-IV): a  $\approx 10$ ms oscillatory approach (I) to the Floquet prethermal plateau (II), followed by unconstrained thermalization (III). Infinite temperature regime (IV) is not reached in these measurements up to 573s. (B) *Semi-log* plot of the experimental data (red points) in regime II-III shows a dynamic change of the thermalization rate. Moving averaging is applied here every 0.1s. Blue line is a fit to a sum of five exponentials. (C) *Semi-log plot against  $\sqrt{t}$*  yields an approximately linear dependence (dashed line) for  $\sim 500$ s. Cusp (marked) at  $\approx 9.2$ ms marks transition to the prethermal plateau (regime II, see also Fig. 5).

toggleing frame Hamiltonians after every pulse [33],  $\mathcal{H}^{(j)} = \exp(ij\vartheta I_x)\mathcal{H}\exp(-ij\vartheta I_x)$ . This evolution can be recast as,  $U(t) = \exp(i\mathcal{H}_F N\tau)$ , where  $\mathcal{H}_F$  is the Floquet Hamiltonian that captures the system dynamics under the drive.  $\mathcal{H}_F$  can be expanded in a Floquet-Magnus expansion [34–36] to leading order in the parameter  $\zeta = \omega/J$ , and in the regime  $\zeta \ll 1$ , yields a time independent Hamiltonian,

$$\mathcal{H}_F^{(0)} = \sum_{j=1}^N \mathcal{H}^{(j)} \approx \sum_{j < k} d_{jk}^{\text{CC}} \left( \frac{3}{2} \mathcal{H}_{\text{ff}} - \vec{I}_j \cdot \vec{I}_k \right), \quad (1)$$

with the flip-flop Hamiltonian,  $\mathcal{H}_{\text{ff}} = I_{jz}I_{kz} + I_{jy}I_{ky}$  [37]. The  $\mathcal{H}_z$  dephasing fields are filtered out in  $\mathcal{H}_F^{(0)}$ . For sufficiently small  $\zeta$ , Eq. (1) holds irrespective of the flip-angle  $\vartheta$ , except for certain special values ( $\vartheta \approx \pi, 2\pi$ ). We note that this constitutes a key difference with respect to conventional dynamical decoupling control (CPMG [38]), wherein the interspin couplings are retained and result in rapid  $^{13}\text{C}$  decay [37]. The higher order terms in the Magnus expansion are progressively smaller, but contribute to long time system dynamics [35, 39]. Importantly, the initial transverse magnetized state  $\rho_I$  is a conserved quantity under  $\mathcal{H}_F^{(0)}$ , since  $[\rho_I, \mathcal{H}_F^{(0)}] = 0$ . This leads to prethermalization of the nuclear spins, with a lifetime that de-

pends exponentially on the drive frequency  $\omega$ . Ultimately, the divergence of the expansion manifests in the system heating to infinite temperature.

Fig. 2C shows the measured survival probability  $F(N\tau)$  of the state  $\rho_I$  under the applied Floquet drive. This can be expressed as,  $F(N\tau) = \frac{1}{2} \text{Tr}\{\rho_I U(N\tau)^\dagger \rho_I U(N\tau)\}$ . We have neglected the first 100ms here for clarity (see Fig. 3A for full data). Data shows significant extension in the transverse state lifetimes. Points in Fig. 2C are the experimental data while the line is a fit to a sum of five exponentials (zoomed in Fig. 2C(ii)); the high measurement SNR is evident in the zoomed data. The product  $J\tau$  is a convenient metric to label the Floquet regime of operation, and in these measurements  $J\tau = 0.066$ . The  $\vartheta \approx \pi/2$  pulses here are applied every  $\tau \approx 100\mu\text{s}$ , and the 573s period encapsulates  $\approx 5.8$ M pulses. For comparison, the conventional  $^{13}\text{C}$  free induction decay [40] in the absence of Floquet driving is shown in Fig. 2A, where decay occurs in  $T_2^* \approx 1.5$ ms on account of internuclear couplings and static field disorder. High SNR allows us to recognize (see Fig. 3B) a dynamic change in the decay rate constant along the curve, making it difficult to quantify the decay rate by a single number. The data especially past 100ms is found to fit well to the stretched exponential  $\sim \exp[-(t/T_2^*)^{1/2}]$ , from where we extract  $T_2^* \approx 353$ s. Alterna-

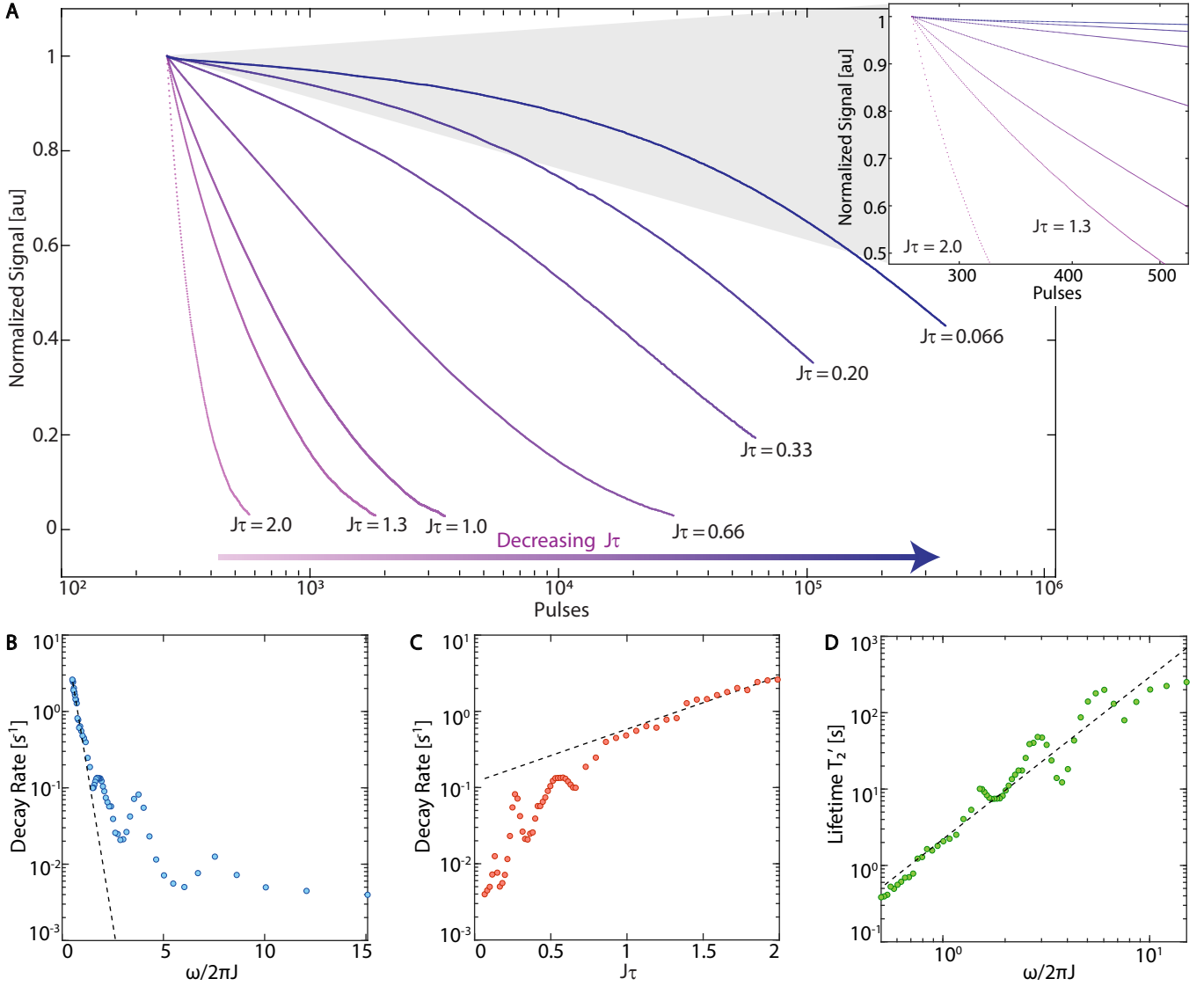


Fig. 4. **Exponential dependence of Floquet prethermal lifetimes.** (A) Variation with  $J\tau$ . Data (points) shows measured signal probing thermalization dynamics in regime **II-III** for representative  $J\tau$  values (colorbar). Here  $\vartheta \approx \pi/2$  and  $t_{\text{acq}} = 32\mu\text{s}$  and there are a high number ( $\sim 10^3$ - $10^6$ ) points per line [31]. Data is normalized at the transition points to the prethermal plateau (following Fig. 3C). The Floquet prethermal decay rates reduce considerably with decreasing  $J\tau$ . See full data at Ref. [32]. *Inset:* Zoom-in (on semilog scale). (B) Extracted decay rates focusing on the region where decay follows  $\sim \exp(-t^{1/2})$ . Plotted in a semi-log scale against  $\omega/J$ , the dashed line reveals an approximately exponential scaling of the decay rates at low drive frequencies  $\omega$  (dashed line is a linear fit). At high  $\omega$  we observe sharp narrow features in the prethermal decay rates. (C) Plotted against  $J\tau$ , showing exponential scaling at higher drive frequency (dashed line). Narrow features in the decay rates superimposed on the exponential background are more emphasized here. (D) Log-scale plot of the extracted  $T_2'$  lifetimes against  $\omega$ . Dashed line is a linear fit.

tively, using an  $1/e$ - intersection (dashed line in Fig. 2C) as a convenient proxy yields,  $T_2' = 90.9\text{s}$ . The extension leads to substantial line-narrowing of the  $^{13}\text{C}$  NMR spectrum ( $\sim 28\text{MHz}$  in Fig. 1C).

Let us now briefly outline the measurement procedure specific to Fig. 2C. The inductive NMR signal from the precessing nuclei, heterodyned to  $f_{\text{het}} = 20\text{MHz}$  (see Fig. 2C(i)) is sampled every 1ns in  $t_{\text{acq}}$  windows between the pulses (see Fig. 2B). Such continuous readout (akin to weak measurement [41]) allows “tracking” of the entire thermalization dynamics in a single measurement run, a significant advantage over point-by-point stroboscopic measurements. The raw data is then digitally band-

pass filtered and amplitude at  $f_{\text{het}}$  extracted; these are the data points plotted in Fig. 2C. The rapid data sampling throughput (at  $f_s = \tau^{-1}$ ) in the decay envelope then allows further filtering to be applied in regions where dynamics are slow compared to  $f_s$ . In particular, we apply moving average (low-pass) filtering over  $\sim 0.1\text{s}$  windows to enhance SNR further (see Supplementary Information [31]). Ultimately, from Fig. 2C, we obtain a single-shot SNR  $> 10^3$  per measurement point, and  $\approx 4 \times 10^9$  for the integrated signal (see Fig. 1C) estimated from the ratio of the peak signal and standard deviation of the noise at the spectral wing. Fourier transformation of the decay envelope yields the  $^{13}\text{C}$  NMR spectrum, shown on a log-scale in Fig. 1C.

**Floquet Prethermalization** – To better illustrate Floquet ther-

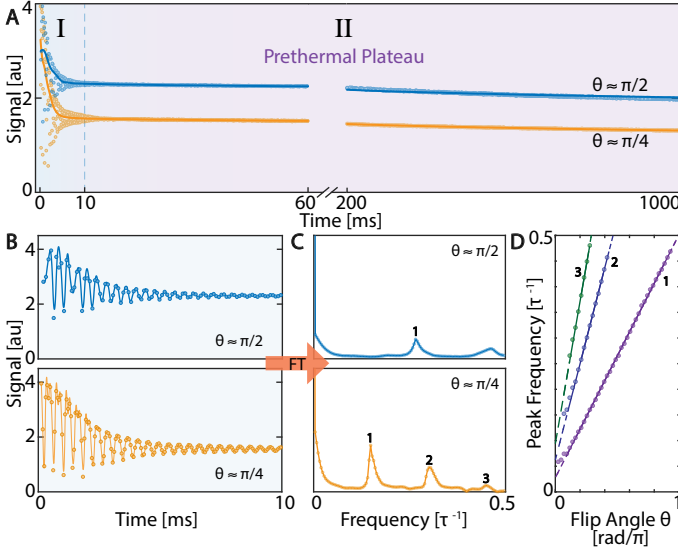


Fig. 5. **Transient approach to prethermal plateau.** (A) Oscillations in the approach to prethermal plateau seen for data zooming in on region I, in a 1s long window (see Fig. 3A). Data (points) corresponds to  $\vartheta \approx \{\pi/2, \pi/4\}$  respectively. Solid line is data with moving average filtering applied over the entire region (see Fig. 3B). (B) Zoom in to region I shows the transient approach with high SNR. It is evident that the oscillations are at higher frequency for  $\vartheta \approx \pi/2$ . Solid line is a spline fit to guide the eye. (C) Fourier transforms of panels in B allows identification of the frequency components constituting the oscillations as a function of  $\omega = \tau^{-1}$ . Harmonics are represented by numbers. It is clear that primary oscillation frequency is higher for  $\vartheta \approx \pi/2$ , where we extract the primary harmonic position at  $\approx 0.26\tau^{-1}$ . (D) Variation with flip angle  $\vartheta$ . Data shows the position of the oscillation frequency for the primary and higher harmonics (numbered). See full data at Ref. [42]. Solid lines are linear fits, while dashed line is an extrapolation. Slopes are in the ratio expected.

malization dynamics of the spins, Fig. 3A shows the full data corresponding to Fig. 3B on a logarithmic time scale. The FID is also shown, and lifetime extension is evident from the shift in the curves. Points are experimental data (no moving average is applied here) and the solid and dashed lines are stretched exponential fits. We identify distinct, albeit smoothly transitioning, regimes in the thermalization process (shaded in Fig. 3A). Following Refs. [2, 9, 14], we refer to them as: (I) an initial regime of constrained thermalization ( $0 < t < 20\text{ms}$ ), where we observe oscillatory behavior with a sub-harmonic frequency response of the Floquet drive frequency  $\omega$ , (II) the Floquet prethermal plateau, leading into (III) unconstrained thermalization towards the (IV) featureless infinite temperature state (not reached in these experiments).

Let us first focus our attention to the dynamics in regimes II and III. Fig. 3B-C shows two complementary visualizations where the points are data and the solid lines are fits. Moving average filtering is applied over the entire data. Fig. 3B, plotted on a semi-log scale, makes evident that the decay rate constant changes over the entire thermalization period. The high SNR and rapid sampling rate, however, allows us to unravel the exact rate change behavior in a manner not accessible in previous experiments. It is easiest seen when replotted against  $\sqrt{t}$  in Fig. 3C, where we obtain an approximately linear trend (dashed line) over a long period ( $\sim 500\text{s}$ ). The prethermal dynamics is

therefore  $\sim \exp(-t^\alpha)$  with exponent  $\alpha \approx 1/2$ . Decades-old NMR experiments had observed a similar trend in paramagnetic impurity rich solids [43, 44]. We emphasize however the high SNR of the data in Fig. 3, proffering insights into, and deviations from, this behavior. At higher  $J\tau$  values, for instance, we observe a dynamic decrease in  $\alpha$  away from  $1/2$  in regime III (see Supplementary Information and Ref. [32]). The turning point (cusp) in data in Fig. 3C, obtained after moving average filtering over the oscillations in regime I, also allows a convenient means to quantify the exact point of transition to Floquet prethermalization. The length of this period ( $\approx 10\text{-}20\text{ms}$ ) closely mirrors the period over which the FID completely decays (see Fig. 3A).

To study the scaling of the prethermal lifetimes with the frequency of the Floquet drive  $\omega$ , Fig. 4A shows similar data at a range of  $J\tau$  values. This is carried out by varying the interpulse spacing  $\tau$  in Fig. 2B. The full dataset (shown in Supplementary Information) consists of measurements at 57 such  $J\tau$  values, but we show a restricted set here for clarity. Again, there is a high density of data points in each experimental line. To restrict attention to regions II-III, we normalize the data at the transition points to the prethermal plateau, identified from the cusps as in Fig. 3C. The data show thermalization proceeding slower for lower values of  $J\tau$ . This is more clearly visible in the inset of Fig. 4A. The dynamic change of rate coefficient makes plotting a single graph that encapsulates the full long-time behavior difficult. Instead, we extract the decay rates focusing on regime II, where decay (similar to Fig. 3C) follows an exponent  $\alpha \approx 1/2$ .

This is presented in three complementary viewpoints in Fig. 4B-D. First, in Fig. 4B plotted on a semi-log scale with respect to the drive frequency  $\omega$ , we see a linear trend in the decay rates, especially at low  $\omega$  (dashed line). This points to an approximately exponential scaling of the state preservation lifetimes with drive frequency, one of the signatures of Floquet prethermalization. At high  $\omega$  however, we observe a flatter slope with sharp features in the decay rates. Fig. 4C shows an alternate view instead in terms of  $J\tau$ , the dashed line once again indicating exponential scaling at high driving. Finally, extracting the transverse state lifetimes  $T_2'$  on a log-log plot in Fig. 4D, we find a strongly exponential dependence with increasing drive frequency.

The sharp peaks in the decay rates in the high  $\omega$  regime in Fig. 4B-D are intriguing. We believe this is a manifestation of quantum sensing — the  $^{13}\text{C}$  nuclei see an enhanced decay rate when subjected to environmental magnetic fields at a fixed frequency  $f_{\text{ac}}$  matched in periodicity (resonant) with the pulse sequence, at  $f_{\text{ac}} = 2\pi/(\vartheta\tau)$ . The first two peaks are for instance at  $f_{\text{ac}} \approx 20.4\text{kHz}$  and  $f_{\text{ac}} \approx 40.8\text{kHz}$ . The exact origin of these fields in Fig. 4B-D are unclear and beyond the scope of the current manuscript. A more detailed exposition on exploiting Floquet prethermal states for quantum sensing will be presented elsewhere.

**Approach to prethermal plateau** – Finally, let us elucidate how the nuclear spins approach the Floquet prethermal plateau [45], focusing attention on the regime I of Fig. 3A. We observe transients in the survival probability leading into the plateau; this is shown for two choices of the flip-angle  $\vartheta$  in Fig. 5A ( $\vartheta \approx \pi/2$  and  $\vartheta \approx \pi/4$ ) respectively. High SNR allows us to track the oscillatory dynamics after every pulse. Points in Fig. 5A are data and the solid line is the data with moving average filtering applied. A cusp is visible similar to Fig. 3B. Moreover, the Floquet prethermal plateau level is it-

self dependent on  $\vartheta$ . The transients last for  $t \approx 10$ ms, which is approximately the total lifetime for the original FID, and is of the order of magnitude of  $\|\mathcal{H}_{dd}\|^{-1}$  (see Fig. 3A). As Fig. 5B indicates, the oscillation periodicity is closely related to the flip angle employed; for  $\vartheta \approx \pi/2$ , for instance, the oscillations occur at a fourth of the frequency of the Floquet drive  $\omega$ . To see this more clearly, Fig. 5C shows the respective Fourier transforms in a 10ms region. Plotted against  $\omega$ , we identify harmonics of the oscillatory dynamics (numbers). For  $\vartheta \approx \pi/4$  (lower panels in Fig. 5B-C), we recognize a primary harmonic and higher harmonics at  $\approx n\omega/8$ , where  $n$  is an integer.

Intuitively, this characteristic periodicity can be thought of as arising from the number of pulses  $N_k$  required to return the Floquet unitary to a prior configuration; *i.e.* such that the toggling frame Hamiltonian after  $2N_k$  pulses is equivalent to that after  $N_k$ ,  $\mathcal{H}^{(2N_k)} = \mathcal{H}^{(N_k)}$ . This corresponds to effectively completing a  $2\pi$  rotation of the Hamiltonian in the toggling frame. Four pulses are therefore needed for  $\vartheta = \pi/2$  in Fig. 5A. In general, the primary harmonic frequency is expected to be at frequency  $f = 2\pi/\vartheta\tau$ . Experiments confirm this picture; in Fig. 5C we extract the oscillation frequencies in regime I as a function of  $\vartheta$ , and they fall neatly onto three straight lines for the three harmonics (see Fig. 5C). We hypothesize that the higher

harmonics arise from bilinear and trilinear terms in the density matrix produced by dipolar evolution. The experimentally measured slopes are in the ratio 1:1.98:2.93, close to the 1:2:3 pattern theoretically expected.

In conclusion, we have observed Floquet prethermalization of dipolar-coupled nuclear spins in a bulk solid at room temperature. The observed  $>90$ s-long prethermal lifetimes in diamond  $^{13}\text{C}$  nuclei are over four orders of magnitude longer than free induction decay times, and significantly longer than in other systems. Our measurements unveil regimes of Floquet thermalization with a high degree of clarity. Apart from fundamental insights, our work points to attractive opportunities possible via Floquet control in hyperpolarizable, dilute and low- $\gamma_n$  nuclear networks. Protection and continuous interrogation of spins along a Bloch transverse axis for  $\sim 10$ min periods opens avenues for high sensitivity magnetometers, gyroscopes [46, 47], and spin sensors [48] constructed out of hyperpolarized prethermal  $^{13}\text{C}$  nuclei.

We gratefully acknowledge M. Markham (Element6) for the diamond sample used in this work, and discussions with S. Bhave, C. Meriles, J. Reimer, D. Sakellariou and A. Souza. This work was funded by ONR under contract N00014-20-1-2806. BG was supported by DOE BES CSGB under contract DE-AC02-05CH11231.

- 
- [1] L. F. Santos, The quick drive to pseudo-equilibrium, *Nature Physics*, 1 (2021).
- [2] L. D'Alessio and M. Rigol, Long-time behavior of isolated periodically driven interacting lattice systems, *Physical Review X* **4**, 041048 (2014).
- [3] N. Goldman and J. Dalibard, Periodically driven quantum systems: effective hamiltonians and engineered gauge fields, *Physical review X* **4**, 031027 (2014).
- [4] M. Bukov, L. D'Alessio, and A. Polkovnikov, Universal high-frequency behavior of periodically driven systems: from dynamical stabilization to floquet engineering, *Advances in Physics* **64**, 139 (2015).
- [5] D. A. Abanin, W. De Roeck, and F. Huveneers, Exponentially slow heating in periodically driven many-body systems, *Physical review letters* **115**, 256803 (2015).
- [6] A. Lazarides, A. Das, and R. Moessner, Equilibrium states of generic quantum systems subject to periodic driving, *Physical Review E* **90**, 012110 (2014).
- [7] M. Bukov, S. Gopalakrishnan, M. Knap, and E. Demler, Prethermal floquet steady states and instabilities in the periodically driven, weakly interacting bose-hubbard model, *Physical review letters* **115**, 205301 (2015).
- [8] D. A. Abanin, W. De Roeck, W. W. Ho, and F. Huveneers, Effective hamiltonians, prethermalization, and slow energy absorption in periodically driven many-body systems, *Physical Review B* **95**, 014112 (2017).
- [9] S. A. Weidinger and M. Knap, Floquet prethermalization and regimes of heating in a periodically driven, interacting quantum system, *Scientific reports* **7**, 1 (2017).
- [10] D. J. Luitz, R. Moessner, S. Sondhi, and V. Khemani, Prethermalization without temperature, *Physical Review X* **10**, 021046 (2020).
- [11] D. V. Else and C. Nayak, Classification of topological phases in periodically driven interacting systems, *Physical Review B* **93**, 201103 (2016).
- [12] V. Khemani, A. Lazarides, R. Moessner, and S. L. Sondhi, Phase structure of driven quantum systems, *Physical review letters* **116**, 250401 (2016).
- [13] H. Zhao, F. Mintert, R. Moessner, and J. Knolle, Random multipolar driving: Tunably slow heating through spectral engineering, *Phys. Rev. Lett.* **126**, 040601 (2021).
- [14] O. Howell, P. Weinberg, D. Sels, A. Polkovnikov, and M. Bukov, Asymptotic prethermalization in periodically driven classical spin chains, *Physical review letters* **122**, 010602 (2019).
- [15] A. Rubio-Abadal, M. Ippoliti, S. Hollerith, D. Wei, J. Rui, S. Sondhi, V. Khemani, C. Gross, and I. Bloch, Floquet prethermalization in a bose-hubbard system, *Physical Review X* **10**, 021044 (2020).
- [16] K. Viebahn, J. Minguzzi, K. Sandholzer, A.-S. Walter, M. Sajani, F. Görg, and T. Esslinger, Suppressing dissipation in a floquet-hubbard system, *Physical Review X* **11**, 011057 (2021).
- [17] M. Ueda, Quantum equilibration, thermalization and prethermalization in ultracold atoms, *Nature Reviews Physics*, 1 (2020).
- [18] P. Peng, C. Yin, X. Huang, C. Ramanathan, and P. Cappellaro, Floquet prethermalization in dipolar spin chains, *Nature Physics*, 1 (2021).
- [19] C. Yin, P. Peng, X. Huang, C. Ramanathan, P. Cappellaro, *et al.*, Prethermal quasiconserved observables in floquet quantum systems, *Physical Review B* **103**, 054305 (2021).
- [20] J. Rovny, R. L. Blum, and S. E. Barrett, Observation of discrete-time-crystal signatures in an ordered dipolar many-body system, *Physical review letters* **120**, 180603 (2018).
- [21] C. L. Degen, F. Reinhard, and P. Cappellaro, Quantum sensing, *Reviews of modern physics* **89**, 035002 (2017).
- [22] E. Reynhardt and C. Terblanche,  $^{13}\text{C}$  relaxation in natural diamond, *Chemical physics letters* **269**, 464 (1997).
- [23] E. C. Reynhardt and G. L. High, Dynamic nuclear polarization of diamond. iii. paramagnetic electron relaxation times from enhanced [sup 13]c nuclear magnetic resonance signals, *The Journal of Chemical Physics* **113**, 744 (2000).
- [24] A. Ajoy, B. Safvati, R. Nazaryan, J. Oon, B. Han, P. Raghavan, R. Nirodi, A. Aguilar, K. Liu, X. Cai, *et al.*, Hyperpolarized

- relaxometry based nuclear  $^1\text{H}$  noise spectroscopy in diamond, *Nature communications* **10**, 1 (2019).
- [25] M. M. Maricq, Spin thermodynamics of periodically time-dependent systems: The quasistationary state and its decay, *Physical Review B* **36**, 516 (1987).
- [26] M. M. Maricq, Long-time limitations of the average hamiltonian theory: A dressed-states viewpoint, in *Advances in Magnetic Resonance: The Waugh Symposium* (Academic Press, 1990) pp. 151–182.
- [27] Y. Dong, R. Ramos, D. Li, and S. Barrett, Controlling coherence using the internal structure of hard  $\pi$  pulses, *Physical review letters* **100**, 247601 (2008).
- [28] D. Hoult, The nmr receiver: a description and analysis of design, *Progress in Nuclear Magnetic Resonance Spectroscopy* **12**, 41 (1978).
- [29] A. Ajoy, K. Liu, R. Nazaryan, X. Lv, P. R. Zangara, B. Safvati, G. Wang, D. Arnold, G. Li, A. Lin, *et al.*, Orientation-independent room temperature optical  $^{13}\text{C}$  hyperpolarization in powdered diamond, *Sci. Adv.* **4**, eaar5492 (2018).
- [30] A. Ajoy, R. Nazaryan, K. Liu, X. Lv, B. Safvati, G. Wang, E. Druga, J. Reimer, D. Suter, C. Ramanathan, *et al.*, Enhanced dynamic nuclear polarization via swept microwave frequency combs, *Proceedings of the National Academy of Sciences* **115**, 10576 (2018).
- [31] See supplementary online material.
- [32] Video showing full dataset of Fig. 4: [https://www.youtube.com/watch?v=uLKIR\\_XM\\_FQ](https://www.youtube.com/watch?v=uLKIR_XM_FQ) (2021).
- [33] U. Haeberlen, *High Resolution NMR in Solids: Selective Averaging* (Academic Press Inc., New York, 1976).
- [34] W. Magnus, On the exponential solution of differential equations for a linear operator, *Communications on Pure and Applied Mathematics* **7**, 649 (1954).
- [35] R. M. Wilcox, Exponential operators and parameter differentiation in quantum physics, *Journal of Mathematical Physics* **8**, 962 (1967).
- [36] S. Blanes, F. Casas, J. Oteo, and J. Ros, The magnus expansion and some of its applications, *Physics Reports* **470**, 151 (2009).
- [37] A. Ajoy, R. Nirodi, A. Sarkar, P. Reshetikhin, E. Druga, A. Akkiraju, M. McAllister, G. Maineri, S. Le, A. Lin, *et al.*, Dynamical decoupling in interacting systems: applications to signal-enhanced hyperpolarized readout, arXiv preprint arXiv:2008.08323 (2020).
- [38] H. Y. Carr and E. M. Purcell, Effects of diffusion on free precession in nuclear magnetic resonance experiments, *Phys. Rev.* **94**, 630 (1954).
- [39] R. Ernst, G. Bodenhausen, and A. Wokaun, *Principles of nuclear magnetic resonance in one and two dimensions* (Clarendon Press Oxford, 1987).
- [40] I. Lowe, Free induction decays of rotating solids, *Physical Review Letters* **2**, 285 (1959).
- [41] M. Pfender, P. Wang, H. Sumiya, S. Onoda, W. Yang, D. B. R. Dasari, P. Neumann, X.-Y. Pan, J. Isoya, R.-B. Liu, *et al.*, High-resolution spectroscopy of single nuclear spins via sequential weak measurements, *Nature communications* **10**, 1 (2019).
- [42] Video showing full dataset of Fig. 5: <https://www.youtube.com/watch?v=8NI7Zzugi4o> (2021).
- [43] D. Tse and S. Hartmann, Nuclear spin-lattice relaxation via paramagnetic centers without spin diffusion, *Physical Review Letters* **21**, 511 (1968).
- [44] N.-a. Lin and S. Hartmann, Nuclear spin-lattice relaxation in  $\text{CaF}_2$  via paramagnetic centers for short correlation time when spin diffusion is inhibited, *Physical Review B* **8**, 4079 (1973).
- [45] A. Haldar, R. Moessner, and A. Das, Onset of floquet thermalization, *Physical Review B* **97**, 245122 (2018).
- [46] A. Ajoy and P. Cappellaro, Stable three-axis nuclear-spin gyroscope in diamond, *Phys. Rev. A* **86**, 062104 (2012).
- [47] M. Ledbetter, K. Jensen, R. Fischer, A. Jarmola, and D. Budker, Gyroscopes based on nitrogen-vacancy centers in diamond, *Physical Review A* **86**, 052116 (2012).
- [48] M. Abobeih, J. Randall, C. Bradley, H. Bartling, M. Bakker, M. Degen, M. Markham, D. Twitchen, and T. Taminiau, Atomic-scale imaging of a  $^{27}\text{Al}$ -nuclear-spin cluster using a quantum sensor, *Nature* **576**, 411 (2019).

## Supplementary Information

### Floquet prethermalization with lifetime exceeding 90s in a bulk hyperpolarized solid

William Beatrez,<sup>1</sup> Otto Janes,<sup>1</sup> Amala Akkiraju,<sup>1</sup> Arjun Pillai,<sup>1</sup> Alexander Oddo,<sup>1</sup> Paul Reshetikhin,<sup>1</sup>

Emanuel Druga,<sup>1</sup> Maxwell McAllister,<sup>1</sup> Mark Elo,<sup>2</sup> Benjamin Gilbert,<sup>3</sup> Dieter Suter,<sup>4</sup> and Ashok Ajoy,<sup>1,5,\*</sup>

<sup>1</sup> Department of Chemistry, University of California, Berkeley, Berkeley, CA 94720, USA. <sup>2</sup> Tabor Electronics Inc. Hatasia 9, Neshar, 3660301, Israel. <sup>3</sup> Energy Geoscience Division, Lawrence Berkeley National Laboratory, Berkeley, CA 94720, USA. <sup>4</sup> Fakultät Physik, Technische Universität Dortmund, D-44221 Dortmund, Germany. <sup>5</sup> Chemical Science Division, Lawrence Berkeley National Laboratory, University of California, Berkeley, Berkeley, CA 94720, USA.

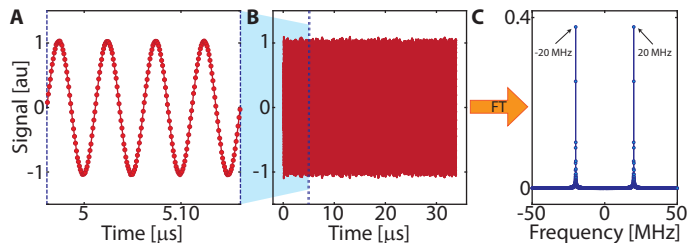


Fig. S1. **Data processing chain.** (A) Raw data of  $^{13}\text{C}$  nuclear precession measured inductively, here heterodyned from 75MHz (Larmor frequency) to 20MHz. The window shown is a 150ns part of the larger acquisition window. (B) Raw data corresponding to one complete acquisition period between the pulses, here  $t_{\text{acq}}=32\mu\text{s}$ . (C) Fourier transformation reveals characteristic peaks at the heterodyning frequency  $\pm 20\text{MHz}$ . This amplitude forms the primary data that is plotted in the main paper. We therefore obtain one data point per acquisition window, and in Fig. 2C a total of  $\approx 5.8\text{M}$  data points.

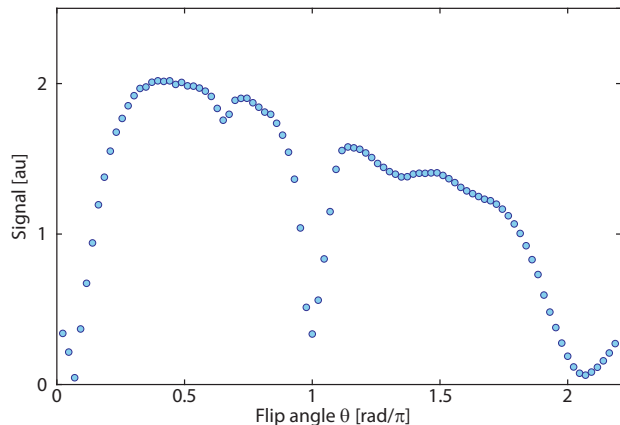


Fig. S2. **Signal dependence on flip angle  $\theta$ .** Panel shows the net signal obtained upon application of a train of  $\theta$ -pulses following the initial  $\pi/2$  pulse. We identify clear signal dips at  $\theta \approx \{\pi, 2\pi\}$  corresponding to rapid decay due to evolution under the dipolar Hamiltonian (see [37]). In these experiments  $t_{\text{acq}}=32\mu\text{s}$  and pulse spacing  $\tau=100\mu\text{s}$ .

## I. DATA PROCESSING

We now present details of the data processing employed in this manuscript. Fig. S1 describes the chain of steps involved in obtaining decay curves such as Fig. 2C of the main paper. We readout the NMR signal continuously in  $t_{\text{acq}}$  periods between the pulses, and the pulses are spaced apart by  $\tau=100\mu\text{s}$ . A representative such acquisition window is shown in Fig. S1B, in this case  $t_{\text{acq}}=32\mu\text{s}$ . The data here (taken 1s into the decay) is sampled at 1Gs/s ( $\Delta t=1\text{ns}$ ). A zoom in (Fig. S1A) reveals high SNR oscillations corresponding to the precession of the hyperpolarized nuclei; the frequency here is 20MHz (heterodyned from the 75MHz Larmor frequency). For each such window, we take a Fourier transform (Fig. S1C), and extract the 20MHz peak. This corresponds effectively to digital bandpass filtering with a filter linewidth of  $\sim t_{\text{acq}}^{-1}$ . Each such point is then plotted to create the decay curves in Fig. 2C, Fig. 3 and Fig. 4. Since the measurements are carried out after every pulse, we obtain a data point in Fig. S1D every  $\tau=100\mu\text{s}$ . Over the 573s decay period, this corresponds to  $\approx 5.8$  million measurement points. However, the data itself is slowly varying (except in regime I), and can be thought of as being effectively oversampled by the measurement points. Moving average filtering thus increases SNR further, acting as a low-pass filter to suppress higher frequency variations. We typically employ a moving average filter size of 0.1s.

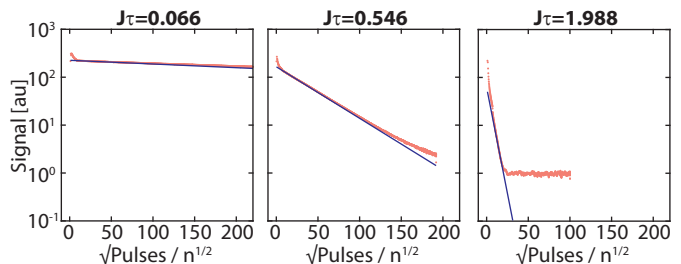


Fig. S3. **Raw data corresponding to Fig. 4** of the main paper. Movie (see at YouTube here:[32]) shows signal plotted on a semi-log scale against  $\sqrt{t}$ . Data are red points, while the blue line is a fit taken in the region where  $\alpha \approx 1/2$ . The extracted rates are plotted as points in the lower panels of Fig. 4 of the main paper.

## II. MATERIALS AND METHODS

The sample used in these experiments consists of a CVD fabricated single crystal of diamond with  $\sim 1\text{ppm}$  of NV centers. The sample is placed flat, i.e. with its [100] face pointing parallel to the hyperpolarization and interrogation magnetic fields (36mT and 7T respectively). In this configuration, the internuclear vector between  $^{13}\text{C}$  nuclei at NN sites on the lattice are positioned at the magic angle, and hence are suppressed.

For hyperpolarization, we employ continuous optical pumping and swept microwave irradiation for  $\sim 40\text{s}$  through a technique described previously. Hyperpolarization is carried out at low field, the sample is shuttled to high field, and the Floquet se-

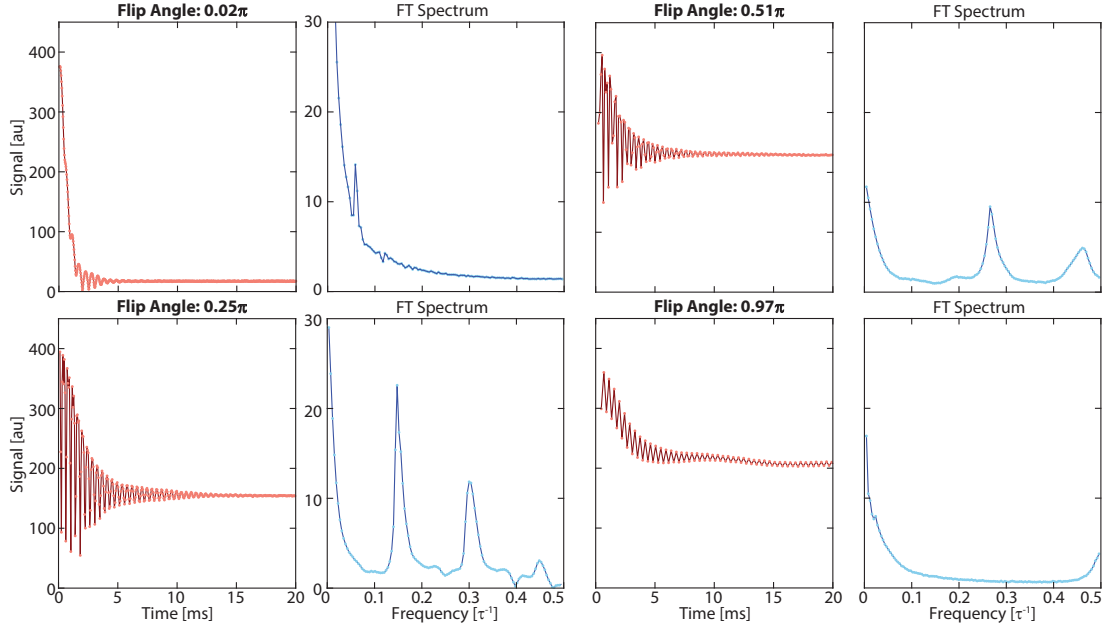


Fig. S4. **Raw data corresponding to Fig. 5** of the main paper. Movie (see at YouTube here:[42]) shows frames corresponding to the transient approach to prethermal plateau for different flip angles  $\vartheta$ . Panels show the transient approach and Fourier transform of the oscillations showing characteristic frequencies.

quence in Fig. 2B is then applied. NV- $^{13}\text{C}$  polarization transfer occurs via biased Landau-Zener traversals in the rotating frame; spin diffusion serves to transfer polarization to bulk  $^{13}\text{C}$  nuclei in the diamond lattice.

Fig. S2 shows the variation of the integrated signal as a function of the flip angle  $\vartheta$  employed in the pulse sequence. We refer the reader to Ref. [37] for a more detailed exposition of the observed trend. For experiments Fig. 2 and Fig. 3 of this paper, we employ a pulse duty cycle of  $\sim 50\%$ , where the measured SNR is highest.

The figure movie Fig. S3 (accessible in Ref. [32]) shows the

full dataset corresponding to Fig. 4 of the main paper. Similar to Fig. 4B, we plot the data against  $\sqrt{t}$  in a semi-log axis. Here the value  $J\tau$  is varied by altering the spacing between the pulses in Fig. 4B. The blue straight lines in the movie show the fit to  $\alpha=1/2$  region. These decay rates, corresponding to the slope of the blue lines in Ref. [32], are plotted in the lower panels of Fig. 4.

Similarly, the figure movie Fig. S4 (accessible in Ref. [42]) shows the full dataset corresponding to Fig. 5 of the main paper, describing the approach to the Floquet prethermal plateau for different values of the flip angle  $\vartheta$ .